ACS Partner Journal
PRECISION CHEMISTRY
pubs.acs.org/PrecisionChem

Letter

HCl Treatment of Mixed-Phase $MoVTeNbO_x$ Catalysts for Enhanced Performance in Selective Oxidation of Propane

Zeyue Wei, Hanzhi Zhang, Yunxing Bai, Xuanyu Zhang, and Weixin Huang*

Cite This: *Precis. Chem.* 2025, 3, 206−213

Read Online

ACCESS | Metrics & More | Article Recommendations | Supporting Information

ABSTRACT: Hydrothermally synthesized mixed-phase $MoVTeNbO_x$ catalysts are active for catalyzing the selective oxidation of propane to acrylic acid but suffer from the presence of the amorphous phase and low specific surface areas. Herein we report that HCl treatment preferentially dissolves the amorphous phase in hydrothermally synthesized mixed-phase $MoVTeNbO_x$ catalysts and increases the catalytic performance. An optimal HCl treatment significantly increases the C_3H_8 conversion from 38.9% to 58.2% without changing the acrylic acid selectivity in the selective oxidation of propane to acrylic acid at 380 °C. The original and HCl treated catalysts exhibit similar apparent activation energies, while HCl treatment increases the specific surface area, surface acid sites, surface V^{5+} density, and C_3H_8 and C_3H_6 irreversible adsorption amounts but decreases the C_3H_8 and C_3H_6 irreversible adsorption heats. The C_3H_8 conversion rate is proportional to the surface V^{5+} density and C_3H_8 irreversible adsorption amount, and the TOF is measured as $3.31 \pm 0.08 \times 10^{-5}$ s^{-1} at 340 °C. Thus, HCl treatment enhances the catalytic performance of mixed-phase $MoVTeNbO_x$ catalysts mainly by increasing the active site density rather than by increasing the active site activity. Our results provide an effective approach to prepare highly active mixed-phase $MoVTeNbO_x$ catalysts for the selective oxidation of propane to acrylic acid.

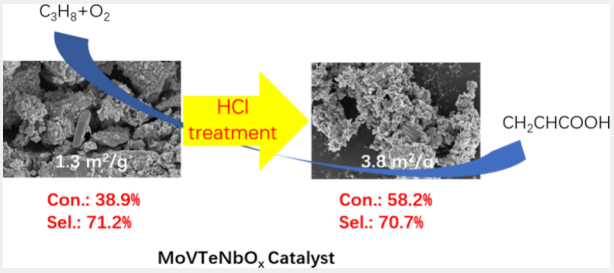

KEYWORDS: *$MoVTeNbO_x$, selective oxidation of propane, acrylic acid, active site, microcalorimetry*

With the shortage of oil and the shale gas revolution,[1] the selective oxidation of propane becomes an alternative to produce acrylic acid, an important chemical widely used to synthesize acrylic paints, acrylic adhesives, superabsorbent polymers, and other products,[2] in addition to the currently adopted two-step propene partial oxidation,[3] in which propene is mainly produced by the intensive energy-consuming and thermodynamically controlled naphtha cracking process.[4,5] To date, $MoVTeNbO_x$ mixed oxide is the most promising catalyst for the selective oxidation of propane to acrylic acid.[6−12] $MoVTeNbO_x$ has the orthorhombic M1 phase and pseudo-hexagonal M2 phase,[13−15] and many strategies, including different synthesis methods,[16−22] doping,[23−29] and modulation of the phase composition,[30−32] were developed to optimize the catalyst performance. An interesting phase synergy between the M1 and M2 phases of $MoVTeNbO_x$ catalysts was observed in the selective oxidation of propane to acrylic acid by mechanical mixtures of the pure phases.[30] We recently found a novel one-pot hydrothermal synthesis assisted by sodium citrate and citric acid to fabricate mixed-phase $MoVTeNbO_x$ catalysts with tunable phase compositions of the M1 and M2 phases to optimize the synergetic effect in catalyzing the selective oxidation of propane to acrylic acid.[33] However, the hydrothermally synthesized mixed-phase $MoVTeNbO_x$ catalysts suffer from the presence of an amorphous phase and low specific surface areas. Herein we report that HCl treatment preferentially dissolves the amorphous phase in hydrothermally synthesized mixed-phase $MoVTeNbO_x$ catalysts and significantly increases the C_3H_8 conversion from 38.9% to 58.2% without changing the acrylic acid selectivity. The active site is precisely identified, and the underlying mechanism is also established.

A mixed-phase $MoVTeNbO_x$ catalyst (denoted as Cat-0) was hydrothermally synthesized using ammonium heptamolybdate, vanadyl sulfate, telluric acid, and ammonium niobium oxalate with an addition of citric acid.[33] Then, Cat-0 was treated in HCl aqueous solutions with concentrations of 3, 6, or 12 wt % at 60 °C for 2 h, respectively, to obtain the catalysts denoted as Cat-3, Cat-6, or Cat-12. Figure 1 compares the catalytic performance of various catalysts in the selective oxidation of propane at different temperatures. At 340 °C, C_3H_8 conversion increases from 18.3% for Cat-0 to 23.1% for Cat-3, 36.0% for Cat-6, and 59.0% for Cat-12, while acrylic acid selectivity is around 70% for Cat-0, Cat-3, and Cat-6 but

Received: November 8, 2024
Revised: January 21, 2025
Accepted: January 21, 2025
Published: January 30, 2025

https://doi.org/10.1021/prechem.4c00089
Precis. Chem. 2025, 3, 206−213

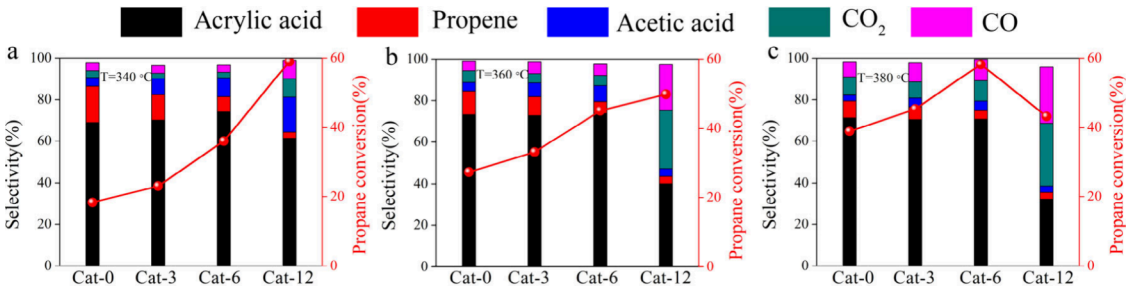

Figure 1. Catalytic performance of Cat-0, Cat-3, Cat-6, and Cat-12 in selective oxidation of propane to acrylic acid at (a) 340, (b) 360, and (c) 380 °C. Reaction conditions: 5% C_3H_8-10% O_2-40% H_2O-45% He, GHSV = 3000 mL g^{-1} h^{-1}.

Table 1. Compositions and Properties of Various MoVTeNbO$_x$ Catalysts

	Cat-0	Cat-3	Cat-6	Cat-12
bulk composition[a]	$MoV_{0.27}Te_{0.26}Nb_{0.20}$	$MoV_{0.28}Te_{0.19}Nb_{0.22}$	$MoV_{0.27}Te_{0.16}Nb_{0.24}$	$MoV_{0.26}Te_{0.11}Nb_{0.28}$
surface composition[b]	$MoV_{0.13}Te_{0.20}Nb_{0.18}$	$MoV_{0.13}Te_{0.20}Nb_{0.18}$	$MoV_{0.12}Te_{0.17}Nb_{0.19}$	$MoV_{0.11}Te_{0.12}Nb_{0.26}$
surface area (m^2/g)	1.3	2.5	3.8	8.7
pore size (nm)	85.6	52.4	49.7	27.9
pore volume (cm^3/g)	0.0107	0.0323	0.0439	0.0606
crystalline size (nm)[c]	33.1	31.7	31.1	29.0
amount and heat of C_3H_8 irreversible adsorption	5.0 μmol/g	6.8 μmol/g	11.1 μmol/g	22.3 μmol/g
	84.7 kJ/mol	74.0 kJ/mol	70.2 kJ/mol	64.3 kJ/mol
amount and heat of C_3H_6 irreversible adsorption	1.8 μmol/g	10.8 μmol/g	20.4 μmol/g	31.1 μmol/g
	99.1 kJ/mol	74.6 kJ/mol	59.6 kJ/mol	46.4 kJ/mol
M1 phase content (wt %)[d]	35.3	44.0	50.2	58.3
M2 phase content (wt %)[d]	19.0	21.1	21.0	26.2
amorphous content (wt %)[d]	45.7	34.9	28.8	15.5
M2/(M2 + M1) (%)	35.0	32.4	29.5	31.0

[a]Measured by ICP-AES. [b]Measured by XPS. [c]Calculated using the (200) diffraction peak at 7.7° of XRD patterns by the Scherrer equation.[36] [d]Phase content calculated from Rietveld refinement analysis of XRD patterns.[35]

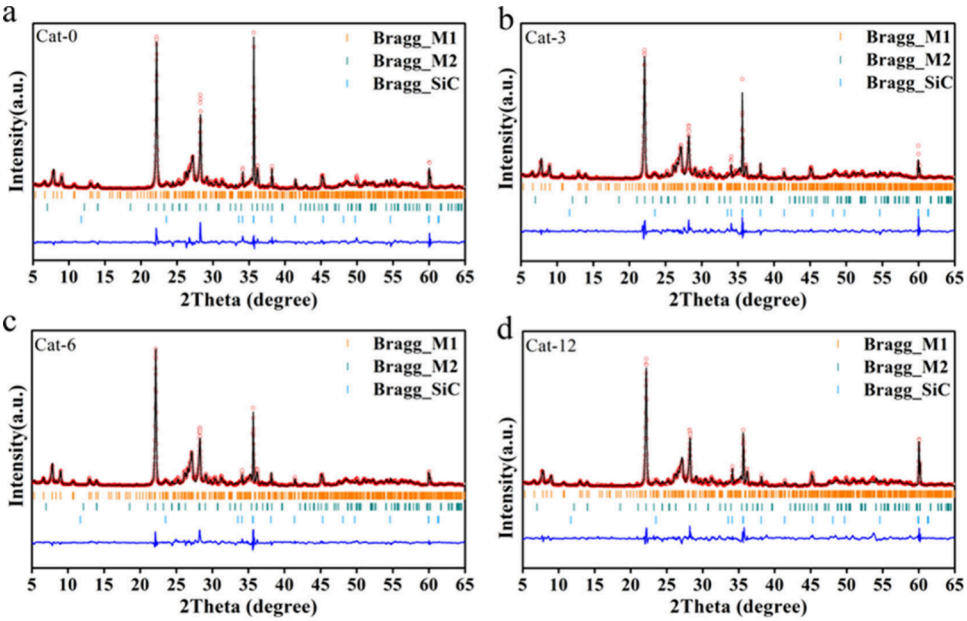

Figure 2. XRD patterns of Cat-0 (a), Cat-3 (b), Cat-6 (c), and Cat-12 (d), refined using the Rietveld method. The catalysts were thoroughly mixed with 20 wt % of a fully crystalline SiC standard material during the XRD measurements to quantify the amorphous content.

61.3% for Cat-12. With the reaction temperature increasing, C_3H_8 conversion increases for Cat-0, Cat-3, and Cat-6, and acrylic acid selectivity remains around 70%. However, C_3H_8 conversion decreases for Cat-12, and CO_x selectivity increases at the expense of acrylic acid selectivity. The different catalytic behavior of Cat-12 from that of the other catalysts results from the full consumption of O_2 that occurred in the selective oxidation of propane catalyzed by Cat-12 already at 360 °C but not for the other catalysts (Figure S1), suggesting the much higher catalytic activity for propane combustion of Cat-12 than

https://doi.org/10.1021/prechem.4c00089
Precis. Chem. 2025, 3, 206−213

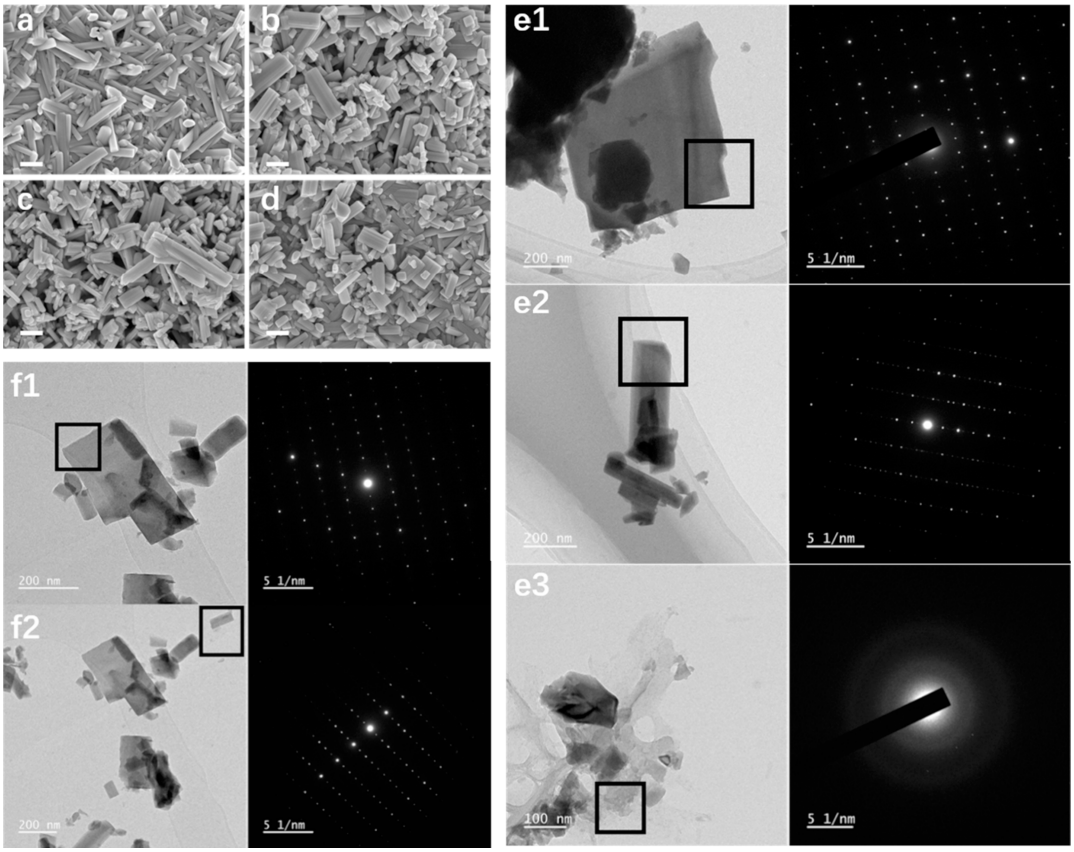

Figure 3. SEM images of Cat-0 (a), Cat-3 (b), Cat-6 (c), and Cat-12 (d). TEM images and selective area electron diffraction patterns (in [010] direction for M1 phase and in [100] direction for M2 phase) of the M2 phase (e1), M1 phase (e2), and amorphous phase (e3) in Cat-0 and the M2 phase (f1) and M1 phase (f2) in Cat-12.

of the other catalysts. These results demonstrate that HCl treatment strongly affects the catalytic performance of hydrothermally synthesized mixed-phase $MoVTeNbO_x$ catalysts in the selective oxidation of propane. An optimal HCl treatment leads to the best Cat-6 catalyst exhibiting a C_3H_8 conversion of 58.2% and an acrylic acid selectivity of 70.7% at 380 °C, better than most previously reported results in the literature (Table S1). Cat-6 also shows good catalytic stability in the selective oxidation of propane at 380 °C (Figure S2). Reaction kinetics of the selective oxidation of propane catalyzed by various catalysts were measured under kinetically controlled reaction conditions (Figure S3). The resulting Arrhenius plots (Figure S4) show that the apparent activation energy is around 85.9 kJ/mol for Cat-0 and slightly increased to around 90.1 kJ/mol for Cat-3, Cat-6, and Cat-9, suggesting that the active site structure is not much affected by HCl treatment.

As summarized in Table 1, the bulk composition is $MoV_{0.27}Te_{0.26}Nb_{0.20}$ for Cat-0, $MoV_{0.28}Te_{0.19}Nb_{0.22}$ for Cat-3, $MoV_{0.27}Te_{0.16}Nb_{0.24}$ for Cat-6, and $MoV_{0.26}Te_{0.11}Nb_{0.28}$ for Cat-12. Thus, the HCl treatment preferentially dissolves Te and then Mo. Phase compositions of various catalysts were quantitatively analyzed using XRD patterns with Rietveld refinement analysis[35] (Figure 2). All catalysts show the diffraction peaks arising from the M1 phase at 6.5°, 7.8°, 8.9°, 22.0°, 27.1°, 35.0°, and 45.0° and from the M2 phase at 22.0°, 28.3°, 36.1°, 45.0°, and 50.1°.[26,37,38] As summarized in Table 1, the M1 phase percentage increases from 35.3% for Cat-0 to 44.0% for Cat-3, 50.2% for Cat-6, and 58.3% for Cat-12, and the M2 phase percentage slightly increases from 19.0% for Cat-0 to around 21.0% for Cat-3 and Cat-6 and to 26.2% for Cat-12. The amorphous phase percentage decreases from 45.7% for Cat-0 to 34.9% for Cat-3, 28.8% for Cat-6, and 15.5% for Cat-12. The M2/(M1 + M2) percentage does not change much, being 35.0%, 32.4%, 29.5% and 31.0% for Cat-0, Cat-3, Cat-6, and Cat-12, respectively. A further quantitative analysis of the mass loss of each phase during HCl treatment (Table S2) demonstrates that the amorphous phase is largely dissolved and the M2 phase is also dissolved, but the M1 phase is barely dissolved. Therefore, HCl treatment preferentially dissolves the amorphous phase in the Cat-0 mixed-phase $MoVTeNbO_x$ catalyst, which is enriched with the Te element.

As summarized in Table 1, the specific surface area increases from 1.3 m^2/g for Cat-0 to 2.5 m^2/g for Cat-3, 3.8 m^2/g for Cat-6, and 8.7 m^2/g for Cat-12. The average pore size keeps decreasing from Cat-0 to Cat-12, while the pore volume keeps increasing. SEM images (Figure 3a–d and Figure S5) display rod-shaped and plate-shaped particles, which are the typical morphologies of M1-phase MoVTeNb oxide and M2-phase MoVTeNb oxide, respectively.[13,39] Size distributions counted from the SEM images of the M1 phase particles in Cat-0 and Cat-12 (Figure S6) show a decrease in the average length from around 231.0 nm for Cat-0 to around 185.6 nm for Cat-12; meanwhile, the average crystalline size of the M1 phase calculated from the XRD patterns[36] (Table 1) shows a gradual decrease from Cat-0 to Cat-12. TEM images of Cat-0 (Figure 3e1–e3) identify the presence of the M1 phase, M2 phase, and amorphous phase, whereas TEM images of Cat-12 (Figure

https://doi.org/10.1021/prechem.4c00089
Precis. Chem. 2025, 3, 206–213

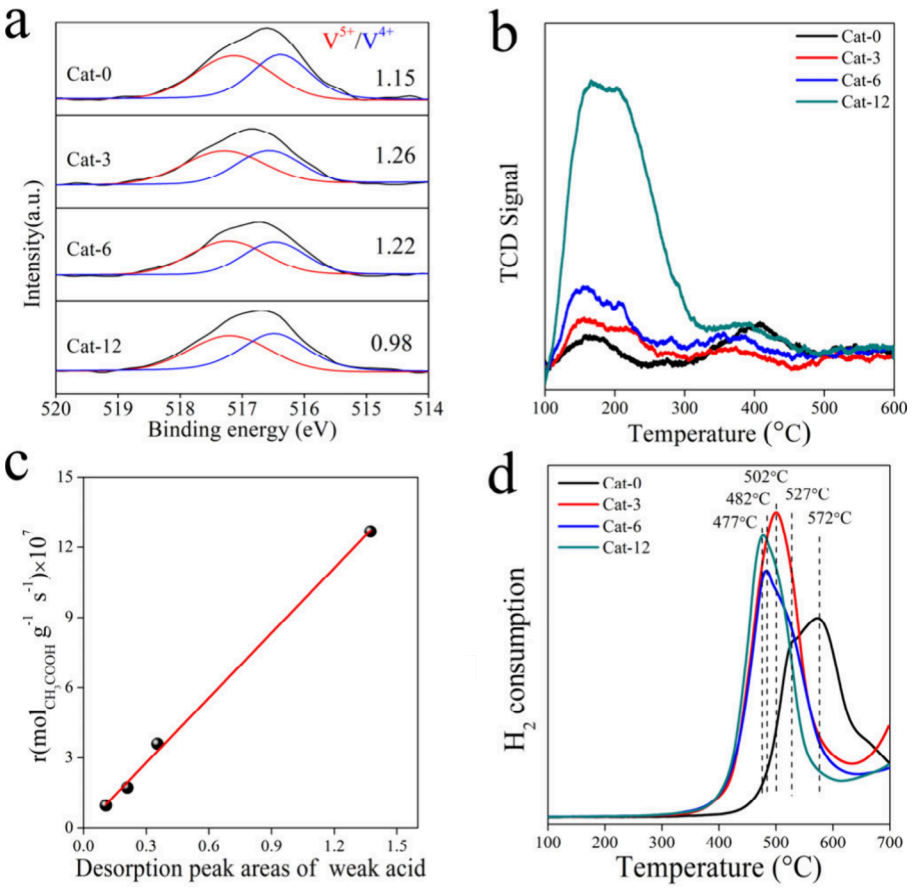

Figure 4. (a) V 2p XPS spectra and (b) NH_3-TPD profiles of various mixed-phase $MoVTeNbO_x$ catalysts. (c) Acetic acid production rate of the selective oxidation of propane catalyzed by various mixed-phase $MoVTeNbO_x$ catalysts as a function of their desorption peak areas of weak acid in the NH_3-TPR profiles. (d) H_2-TPR profiles of various mixed-phase $MoVTeNbO_x$ catalysts.

3f1,f2) mainly identify the presence of the M1 phase and M2 phase, supporting the preferential dissolution of the amorphous phase by HCl treatment. The TEM images also show that the particle sizes of the M1 phase and M2 phase in Cat-0 are larger than those in Cat-12. All these results demonstrate that HCl treatment of Cat-0 decreases the particle size of the M1 phase and M2 phase, which contributes to the increase of catalyst surface area, beneficial for the catalytic activity.

Surface compositions of various mixed-phase $MoVTeNbO_x$ catalysts were characterized using XPS as $MoV_{0.13}Te_{0.20}Nb_{0.18}$ for Cat-0, $MoV_{0.13}Te_{0.20}Nb_{0.18}$ for Cat-3, $MoV_{0.12}Te_{0.17}Nb_{0.19}$ for Cat-6, and $MoV_{0.11}Te_{0.12}Nb_{0.26}$ for Cat-12 (Table 1). Compared to the surface content of Mo, HCl treatment slightly decreases the surface contents of V and Te and increases the surface content of Nb in Cat-3 and Cat-6 but significantly decreases the surface content of Te and increases the surface content of Nb in Cat-12. The Mo 3d, Nb 3d, and Te 3d XPS spectra (Figure S7a–c) all exhibit a single component with the binding energies of Mo $3d_{5/2}$, Nb $3d_{5/2}$, and Te $3d_{5/2}$ features at 232.9 ± 0.2, 207.2 ± 0.2, and 576.5 ± 0.1 eV, respectively, suggesting the presence of Mo^{6+}, Nb^{5+}, and Te^{4+} cations in all catalysts.[30,41−45] No Cl signals were observed in the Cl 2p XPS spectra (Figure S7d). Two components were well resolved in the V 2p XPS spectra with the V $2p_{3/2}$ binding energies at 561.3 and 571.1 eV, respectively, arising from V^{4+} and V^{5+} cations (Figure 4a).[36,46,47] The calculated surface V^{5+}/V^{4+} ratio is 1.15 for Cat-0, 1.26 for Cat-3, 1.22 for Cat-6, and 0.98 for Cat-12. Thus, HCl treatment affects the surface V^{5+}/V^{4+} ratio of various catalysts, while the surface V^{5+} site is considered as the active site on M1-phase $MoVTeNbO_x$ catalysts for propane activation.[14,48,49]

The surface acidity of various catalysts was probed by NH_3-TPD (Figure 4b). The two NH_3 desorption peaks observed at around 150 and 400 °C in the NH_3-TPD spectrum of Cat-0 could be assigned to the weak and strong acid sites, respectively.[21] HCl treatment greatly increases the amount of weak acid sites but seldom increases the amount of strong acid sites, particularly for Cat-12. The enhancement of weak surface acid sites in various catalysts seems to be related to the increasing surface content of Nb. Consistent with a previous report that weak acid sites on $MoVTeNbO_x$ catalysts favored the undesired C−C bond breaking reactions in the selective oxidation of propane, leading to the production of acetic acid and carbon oxides,[40] the production of acetic acid over various mixed-phase MoVTeNb catalysts correlates linearly with the integrated peak area of the NH_3 desorption peak from the weak acid sites (Figure 4c).

The reducibility of various mixed-phase $MoVTeNbO_x$ catalysts was also examined by using H_2-TPR (Figure 4d). Cat-0 exhibits two obvious reduction peaks at around 527 and 572 °C arising from the reduction of the M1 phase and M2 phase, respectively,[33] while Cat-3, Cat-6, and Cat-12 exhibit a dominant reduction peak at around 502, 482, and 477 °C, respectively. These observations suggest that HCl treatment

https://doi.org/10.1021/prechem.4c00089
Precis. Chem. 2025, 3, 206−213

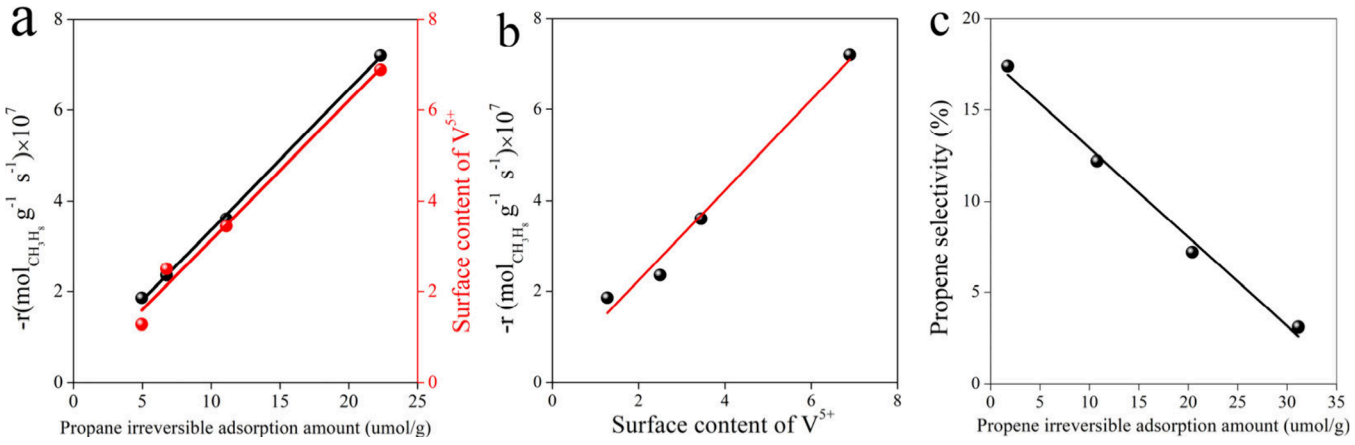

Figure 5. (a) Reaction rate of propane at the temperature of 340 °C and surface content of V^{5+} (surface content of V^{5+} = surface area × surface atomic percentage of V^{5+}) as a function of the irreversible adsorption amount of propane on various mixed-phase $MoVTeNbO_x$ catalysts. (b) Reaction rate of propane at the temperature of 340 °C as a function of the surface content of V^{5+} (surface content of V^{5+} = surface area × surface atomic percentage of V^{5+}) and (c) propene selectivity at the temperature of 340 °C as a function of the irreversible adsorption amount of propene on various mixed-phase $MoVTeNbO_x$ catalysts.

not only significantly promotes the reducibility of the M1 phase in the catalysts, beneficial for the catalytic activity, but also improves the M1−M2 phase synergy in the catalysts, beneficial for the acrylic acid selectivity.

Adsorptions of C_3H_8, the reactant, and C_3H_6, a primary product, on various catalysts at −30 °C were quantitatively studied using flow-adsorption microcalorimetry.[34,50−53] As shown in Figures S8−S11 and summarized in Table 1, the irreversible C_3H_8 adsorption heat and amount are respectively around 84.7 kJ/mol and 5.0 μmol_{C3H8}/g (3.85 $\mu mol_{C3H8}/m^2$) on Cat-0, 74.0 kJ/mol and 6.8 μmol_{C3H8}/g (2.72 $\mu mol_{C3H8}/m^2$) on Cat-3, 70.2 kJ/mol and 11.1 μmol_{C3H8}/g (2.92 $\mu mol_{C3H8}/m^2$) on Cat-6, and 64.3 kJ/mol and 22.3 μmol_{C3H8}/g (2.56 $\mu mol_{C3H8}/m^2$) on Cat-12, while the irreversible C_3H_6 adsorption heat and amount are respectively around 99.1 kJ/mol and 1.8 μmol_{C3H6}/g (1.38 $\mu mol_{C3H6}/m^2$) on Cat-0, 74.6 kJ/mol and 10.8 μmol_{C3H6}/g (4.32 $\mu mol_{C3H6}/m^2$) on Cat-3, 59.6 kJ/mol and 20.4 μmol_{C3H6}/g (5.37 $\mu mol_{C3H6}/m^2$) on Cat-6, and 46.4 kJ/mol and 31.1 μmol_{C3H6}/g (3.57 $\mu mol_{C3H6}/m^2$) on Cat-12. The different adsorption heats of C_3H_8 and C_3H_6 on various catalysts directly prove that HCl treatment alters their surface structures, which could be correlated to the observed surface acidity changes. The mass-specific adsorption amounts of C_3H_8 and C_3H_6 keep increasing from Cat-0 to Cat-3, Cat-6, and Cat-12 due to the increased BET surface areas. However, the surface area-specific adsorption amounts of C_3H_8 of Cat-3, Cat-6, and Cat-12 are smaller than that of Cat-0, whereas their surface area-specific adsorption amounts of C_3H_6 are larger than that of Cat-0. These results support our previous results, which demonstrated that C_3H_8 only adsorbed on the M1 phase of the mixed-phase $MoVTeNbO_x$ catalysts, while C_3H_6 adsorbed on both the M1 phase and the M2 phase.[33] Meanwhile, they also indicate that the surface area increases of Cat-0 upon HCl treatment result from the surface area increases of both the M1 phase and the M2 phase and that the extent of the surface area increase of the M1 phase should be less than that of the M2 phase.

Although the adsorption heat of C_3H_8 varies, the apparent activation energies of the C_3H_8 conversion catalyzed by different mixed-phase catalysts are similar. This supports that the catalyzed selective oxidation of C_3H_8 follows an Mvk mechanism,[33] in which the reactivity of surface lattice oxygen of a mixed-phase $MoVTeNbO_x$ catalyst determines the intrinsic catalytic activity. The mass-specific C_3H_8 conversion rates at 340 °C were acquired under the kinetic-controlled regime (Figure S3) for the selective oxidation of C_3H_8 catalyzed by various mixed-phase $MoVTeNbO_x$ catalysts. They were found to positively linearly correlate with both the surface V^{5+} amount, represented by the surface V^{5+} atomic percentage derived from XPS multiplied by the surface area, and the mass-specific adsorption amount of C_3H_8 (Figure 5a,b). This demonstrates that the surface V^{5+} site on M1-phase $MoVTeNbO_x$ catalysts is the active site for C_3H_8 adsorption and activation and further proves that the different apparent catalytic activity of various mix-phase $MoVTeNbO_x$ catalysts results from the different active site density, not from the active site activity. Taking the irreversible C_3H_8 adsorption amount as the active site density, the TOF in the selective C_3H_8 oxidation reaction at 340 °C was then calculated as 3.48×10^{-5}, 3.31×10^{-5}, 3.21×10^{-5}, and 3.25×10^{-5} s^{-1} for Cat-0, Cat-3, Cat-6, and Cat-12, respectively, giving an average TOF of 3.31×10^{-5} s^{-1}. Despite the very different C_3H_6 irreversible adsorption heats, the mass-normalized C_3H_6 irreversible C_3H_6 adsorption amount on various catalysts was found to negatively linearly correlate with the selectivity of C_3H_6 (Figure 5c). This suggests that the C_3H_6 adsorption amount, rather than the C_3H_6 adsorption heat (binding strength), is responsible for further conversions of adsorbed C_3H_6 on the catalysts.

In summary, we have successfully developed an effective approach of HCl treatment to significantly enhance the catalytic performance of hydrothermally synthesized mixed-phase $MoVTeNbO_x$ catalysts in the selective oxidation of propane to acrylic acid. An optimal HCl treatment significantly increases the C_3H_8 conversion from 38.9% to 58.2% without changes in the acrylic acid selectivity (around 71.0%) in the selective oxidation of propane to acrylic acid at 380 °C. HCl treatment preferentially dissolves the Te-containing amorphous phase in the mixed-phase $MoVTeNbO_x$ catalysts and increases the surface areas of both the M1 phase and the M2 phase, the surface V^{5+}/V^{4+} ratios, and the C_3H_8 irreversible adsorption amounts. These lead to increased active site (surface V^{5+} sites on the M1 phase) densities on mixed-phase $MoVTeNbO_x$ catalysts for C_3H_8 adsorption and

https://doi.org/10.1021/prechem.4c00089
Precis. Chem. 2025, 3, 206−213

activation, resulting in significantly enhanced C_3H_8 conversions.

■ ASSOCIATED CONTENT

Supporting Information

The Supporting Information is available free of charge at https://pubs.acs.org/doi/10.1021/prechem.4c00089.

Experimental section, oxygen conversions of the catalytic reaction, stability test, summary of catalytic performance, reaction kinetic measurements and Arrhenius plots for propane reaction rate, mass loss and phase loss during HCl treatment, SEM images, length distributions of M1 particles, XPS spectra, and microcalorimetric measurements of C_3H_8 and C_3H_6 adsorptions (PDF)

■ AUTHOR INFORMATION

Corresponding Author

Weixin Huang − *State Key Laboratory of Precision and Intelligent Chemistry, iChEM, Key Laboratory of Surface and Interface Chemistry and Energy Catalysis of Anhui Higher Education Institutes and Department of Chemical Physics, University of Science and Technology of China, Hefei 230026, P. R. China;* orcid.org/0000-0002-5025-3124; Email: huangwx@ustc.edu.cn

Authors

Zeyue Wei − *State Key Laboratory of Precision and Intelligent Chemistry, iChEM, Key Laboratory of Surface and Interface Chemistry and Energy Catalysis of Anhui Higher Education Institutes and Department of Chemical Physics, University of Science and Technology of China, Hefei 230026, P. R. China*

Hanzhi Zhang − *State Key Laboratory of Precision and Intelligent Chemistry, iChEM, Key Laboratory of Surface and Interface Chemistry and Energy Catalysis of Anhui Higher Education Institutes and Department of Chemical Physics, University of Science and Technology of China, Hefei 230026, P. R. China*

Yunxing Bai − *State Key Laboratory of Precision and Intelligent Chemistry, iChEM, Key Laboratory of Surface and Interface Chemistry and Energy Catalysis of Anhui Higher Education Institutes and Department of Chemical Physics, University of Science and Technology of China, Hefei 230026, P. R. China*

Xuanyu Zhang − *State Key Laboratory of Precision and Intelligent Chemistry, iChEM, Key Laboratory of Surface and Interface Chemistry and Energy Catalysis of Anhui Higher Education Institutes and Department of Chemical Physics, University of Science and Technology of China, Hefei 230026, P. R. China*

Complete contact information is available at: https://pubs.acs.org/10.1021/prechem.4c00089

Author Contributions

All authors have given approval to the final version of the manuscript.

Notes

The authors declare no competing financial interest.

■ ACKNOWLEDGMENTS

This work was financially supported by the National Key R&D Program of MOST (2021YFA1501301), the Strategic Priority Research Program of the Chinese Academy of Sciences (XDB0450102), the National Natural Science Foundation of China (22202189), and the Changjiang Scholars Program of Ministry of Education of China. This work was partially carried out at the Instruments Center for Physical Science, University of Science and Technology of China.

■ REFERENCES

(1) Li, X.; Pei, C.; Gong, J. Shale Gas Revolution: Catalytic Conversion of C_1-C_3 Light Alkanes to Value-Added Chemicals. *Chem.* **2021**, *7*, 1755−1801.

(2) Vedrine, J. C. Heterogeneous Catalytic Partial Oxidation of Lower Alkanes (C_1-C_6) on Mixed Metal Oxides. *J. Energy Chem.* **2016**, *25*, 936−946.

(3) Valente, J. S.; Quintana-Solorzano, R.; Armendariz-Herrera, H.; Millet, J.-M. M. Decarbonizing Petrochemical Processes: Contribution and Perspectives of the Selective Oxidation of C_1-C_3 Paraffins. *ACS Catal.* **2023**, *13*, 1693−1716.

(4) Monai, M.; Gambino, M.; Wannakao, S.; Weckhuysen, B. M. Propane to Olefins Tandem Catalysis: A Selective Route towards Light Olefins Production. *Chem. Soc. Rev.* **2021**, *50*, 11503−11529.

(5) Chen, S.; Chang, X.; Sun, G.; Zhang, T.; Xu, Y.; Wang, Y.; Pei, C.; Gong, J. Propane Dehydrogenation: Catalyst Development, New Chemistry, and Emerging Technologies. *Chem. Soc. Rev.* **2021**, *50*, 3315−3354.

(6) Lin, M. M. Selective Oxidation of Propane to Acrylic Acid with Molecular Oxygen. *Appl. Catal. A: Gen.* **2001**, *207*, 1−16.

(7) Lintz, H. G.; Müller, S. P. The Partial Oxidation of Propane on Mixed Metal Oxides-A Short Overview. *Appl. Catal. A: Gen.* **2009**, *357*, 178−183.

(8) Tu, X.; Niwa, M.; Arano, A.; Kimata, Y.; Okazaki, E.; Nomura, S. Controlled Silylation of MoVTeNb Mixed Oxide Catalyst for the Selective Oxidation of Propane to Acrylic Acid. *Appl. Catal. A: Gen.* **2018**, *549*, 152−160.

(9) Tian, H.; Xu, B. Kinetic Insights into Boron-Based Materials Catalyzed Oxidative Dehydrogenation of Light Alkanes. *Precis. Chem.* **2024**, *2*, 182−192.

(10) Wang, Y.; Wei, Z.; Zhang, X.; Huang, W. Optimizing Lattice Oxygen Mobility and Acidity of Heteropoly Acid Catalysts for Oxidation of Isobutane to Methacrylic Acid. *Appl. Catal. A: Gen.* **2023**, *649*, 118974.

(11) Wang, Y.; Sun, X.; Wei, Z.; Zhang, X.; Huang, W. Photothermal Catalytic Selective Oxidation of Isobutane to Methacrylic Acid over Keggin-Type Heteropolyacid. *Chin. J. Chem. Phys.* **2023**, *36*, 497−502.

(12) Li, D.; Bi, J.; Xie, Z.; Kong, L.; Liu, B.; Fan, X.; Xiao, X.; Miao, Y.; Zhao, Z. Flour-Derived Borocarbonitride Enriched with Boron-Oxygen Species for the Oxidative Dehydrogenation of Propane to Olefins. *Sci. China Chem.* **2023**, *66*, 2389−2399.

(13) DeSanto, P.; Buttrey, D. J.; Grasselli, R. K.; Lugmair, C. G.; Volpe, A. F.; Toby, B. H.; Vogt, T. Structural Aspects of the M1 and M2 Phases in MoVNbTeO Propane Ammoxidation Catalysts. *Z. Krist - Cryst. Mater.* **2004**, *219*, 152−165.

(14) Grasselli, R. K.; Buttrey, D. J.; Burrington, J. D.; Andersson, A.; Holmberg, J.; Ueda, W.; Kubo, J.; Lugmair, C. G.; Volpe, A. F. Active Centers, Catalytic Behavior, Symbiosis and Redox Properties of MoV(Nb,Ta)TeO Ammoxidation Catalysts. *Top. Catal.* **2006**, *38*, 7−16.

(15) Chen, Y.; Yan, B.; Cheng, Y. State-of-the-Art Review of Oxidative Dehydrogenation of Ethane to Ethylene over $MoVNbTeO_x$ Catalysts. *Catalysts* **2023**, *13*, 204−232.

(16) Deniau, B.; Bergeret, G.; Jouguet, B.; Dubois, J. L.; Millet, J. M. M. Preparation of Single M1 Phase MoVTe(Sb)NbO Catalyst: Study

of the Effect of M2 Phase Dissolution on the Structure and Catalytic Properties. *Top. Catal.* **2008**, *50*, 33−42.
(17) Ramli, I.; Botella, P.; Ivars, F.; Pei Meng, W.; Zawawi, S. M. M.; Ahangar, H. A.; Hernández, S.; Nieto, J. M. L. Reflux Method as a Novel Route for the Synthesis of MoVTeNbOx Catalysts for Selective Oxidation of Propane to Acrylic Acid. *J. Mol. Catal. A: Chem.* **2011**, *342-343*, 50−57.
(18) Kolen'ko, Y. V.; Amakawa, K.; D'alnoncourt, R. N.; Girgsdies, F.; Weinberg, G.; Schlögl, R.; Trunschke, A. Unusual Phase Evolution in MoVTeNb Oxide Catalysts Prepared by a Novel Acrylamide-Gelation Route. *ChemCatChem.* **2012**, *4*, 495−503.
(19) Fan, Y.; Li, S.; Liu, Y.; Wang, Y.; Wang, Y.; Chen, Y.; Yu, S. High-Pressure Hydrothermal Synthesis of $MoVTeNbO_x$ with High Surface V^{5+} Abundance for Oxidative Conversion of Propane to Acrylic Acid. *J. Supercrit. Fluids* **2022**, *181*, 105469−105480.
(20) Shiju, N. R.; Guliants, V. V. Microwave-Assisted Hydrothermal Synthesis of Monophasic Mo-V-Te-Nb-O Mixed Oxide Catalyst for the Selective Ammoxidation of Propane. *ChemPhysChem* **2007**, *8*, 1615−1617.
(21) Li, S.; Liu, Y.; Fan, Y.; Lu, Z.; Yan, Y.; Deng, L.; Zhang, Z.; Yu, S. Facile Sub-/Supercritical Water Synthesis of Nanoflake MoVTeNbO$_x$-Mixed Metal Oxides without Post-Heat Treatment and Their Catalytic Performance. *RSC Adv.* **2020**, *10*, 39922−39930.
(22) Massó-Ramírez, A.; Ivars-Barceló, F.; López-Nieto, J. M. Optimizing reflux Synthesis Method of Mo-V-Te-Nb Mixed Oxide Catalysts for Light Alkane Selective Oxidation. *Catal. Today* **2020**, *356*, 322−329.
(23) Grasselli, R. K.; Lugmair, C. G.; Volpe, A. F. Doping of MoVNbTeO (M1) and MoVTeO (M2) Phases for Selective Oxidation of Propane and Propylene to Acrylic Acid. *Top. Catal.* **2008**, *50*, 66−73.
(24) Deniau, B.; Millet, J. M. M.; Loridant, S.; Christin, N.; Dubois, J. L. Effect of Several Cationic Substitutions in the M1 Active Phase of the MoVTeNbO Catalysts Used for the Oxidation of Propane to Acrylic Acid. *J. Catal.* **2008**, *260*, 30−36.
(25) Ishchenko, E. V.; Kardash, T. Y.; Gulyaev, R. V.; Ishchenko, A. V.; Sobolev, V. I.; Bondareva, V. M. Effect of K and Bi Doping on the M1 Phase in MoVTeNbO Catalysts for Ethane Oxidative Conversion to Ethylene. *Appl. Catal. A: Gen.* **2016**, *514*, 1−13.
(26) Yun, Y. S.; Lee, M.; Sung, J.; Yun, D.; Kim, T. Y.; Park, H.; Lee, K. R.; Song, C. K.; Kim, Y.; Lee, J.; Seo, Y. J.; Song, I. K.; Yi, J. Promoting Effect of Cerium on MoVTeNb Mixed Oxide Catalyst for Oxidative Dehydrogenation of Ethane to Ethylene. *Appl. Catal. B: Environ.* **2018**, *237*, 554−562.
(27) Biswas, P.; Woo, J.; Guliants, V. V. Ruthenium and Gold-Doped M1 Phase MoVNbTeO Catalysts for Propane Ammoxidation to Acrylonitrile. *Catal. Commun.* **2010**, *12*, 58−63.
(28) Xu, A.; Wang, Y.; Ge, H.; Chen, S.; Li, Y.; Lu, W. An Outstanding Cr-Doped Catalyst for Selective Oxidation of Propane to Acrylic Acid. *Chin. J. Catal.* **2013**, *34*, 2183−2191.
(29) Quintana-Solórzano, R.; Mejía-Centeno, I.; Armendáriz-Herrera, H.; Ramírez-Salgado, J.; Rodríguez-Hernandez, A.; Guzmán-Castillo, M. L.; Lopez Nieto, J. M.; Valente, J. S. Discerning the Metal Doping Effect on Surface Redox and Acidic Properties in a $MoVTeNbO_x$ for Propa(E)Ne Oxidation. *ACS Omega* **2021**, *6*, 15279−15291.
(30) Baca, M.; Aouine, M.; Dubois, J. L.; Millet, J. M. M. Synergetic Effect Between Phases in MoVTe(Sb)NbO Catalysts Used for the Oxidation of Propane into Acrylic Acid. *J. Catal.* **2005**, *233*, 234−241.
(31) Baca, M.; Pigamo, A.; Dubois, J. L.; Millet, J. M. M. Propane Oxidation on MoVTeNbO Mixed Oxide Catalysts: Study of the Phase Composition of Active and Selective Catalysts. *Top. Catal.* **2003**, *23*, 39−46.
(32) Ishchenko, E. V.; Popova, G. Y.; Kardash, T. Y.; Ishchenko, A. V.; Plyasova, L. M.; Andrushkevich, T. V. Role of MoVTeNb Oxide Catalyst Constituent Phases in Propane Oxidation to Acrylic Acid. *Catal. Sustain. Energy* **2013**, *1*, 75−81.
(33) Wei, Z.; Zhang, H.; Bai, Y.; Zhang, X.; Huang, W. One-Pot Synthesis of Mixed-Phase $MoVTeNbO_x$ Catalysts for Selective Oxidation of Propane to Acrylic Acid. *J. Phys. Chem. Lett.* **2024**, *15*, 11209−11216.
(34) You, R.; Li, Z.; Zeng, H.; Huang, W. A Flow-Pulse Adsorption-Microcalorimetry System for Studies of Adsorption Processes on Powder Catalysts. *Rev. Sci. Instrum.* **2018**, *89*, 064101.
(35) Valente, J. S.; Armendáriz-Herrera, H.; Quintana-Solórzano, R.; del Angel, P.; Nava, N.; Massó, A.; López-Nieto, J. M. Chemical, Structural, and Morphological Changes of a MoVTeNb Catalyst During Oxidative Dehydrogenation of Ethane. *ACS Catal.* **2014**, *4*, 1292−1301.
(36) Chu, B.; Truter, L.; Nijhuis, T. A.; Cheng, Y. Performance of Phase-Pure M1MoVNbTeO$_x$ Catalysts by Hydrothermal Synthesis with Different Post-Treatments for the Oxidative Dehydrogenation of Ethane. *Appl. Catal. A: Gen.* **2015**, *498*, 99−106.
(37) Chu, B.; An, H.; Nijhuis, T.A.; Schouten, J. C.; Cheng, Y. A Self-Redox Pure-Phase M1MoVNbTeO$_x$/CeO_2 Nanocomposite as a Highly Active Catalyst for Oxidative Dehydrogenation of Ethane. *J. Catal.* **2015**, *329*, 471−478.
(38) Ivars, F.; Solsona, B.; Hernández, S.; López-Nieto, J. M. Influence of Gel Composition in the Synthesis of MoVTeNb Catalysts over Their Catalytic Performance in Partial Propane and Propylene Oxidation. *Catal. Today* **2010**, *149*, 260−266.
(39) Celaya-Sanfiz, A.; Hansen, T. W.; Sakthivel, A.; Trunschke, A.; Schlögl, R.; Knoester, A.; Brongersma, H. H.; Looi, M. H.; Hamid, S. B. A. How Important is the (001) Plane of M1 for Selective Oxidation of Propane to Acrylic Acid ? *J. Catal.* **2008**, *258*, 35−43.
(40) Hävecker, M.; Wrabetz, S.; Kröhnert, J.; Csepei, L. I.; Naumann d'Alnoncourt, R.; Kolen'ko, Y. V.; Girgsdies, F.; Schlögl, R.; Trunschke, A. Surface Chemistry of Phase-Pure M1MoVTeNb Oxide During Operation in Selective Oxidation of Propane to Acrylic Acid. *J. Catal.* **2012**, *285*, 48−60.
(41) Heine, C.; Hävecker, M.; Trunschke, A.; Schlögl, R.; Eichelbaum, M. The Impact of Steam on the Electronic Structure of the Selective Propane Oxidation Catalyst MoVTeNb Oxide (Orthorhombic M1 Phase). *Phys. Chem. Chem. Phys.* **2015**, *17*, 8983−8993.
(42) Dang, D.; Chen, X.; Yan, B.; Li, Y. K.; Cheng, Y. Catalytic Performance of Phase-Pure M1MoVNbTeO$_x$/CeO_2 Composite for Oxidative Dehydrogenation of Ethane. *J. Catal.* **2018**, *365*, 238−248.
(43) Chen, Y.; Yan, B.; Cheng, Y. Microporous Exposure on Catalytic Performance of $MoVNbTeO_x$ Mixed Metal Oxides in the Oxidative Dehydrogenation of Ethane. *J. Catal.* **2023**, *426*, 308−318.
(44) Deniau, B.; Nguyen, T. T.; Delichere, P.; Safonova, O.; Millet, J.-M. M. Redox State Dynamics at the Surface of MoVTe(Sb)NbO M1 Phase in Selective Oxidation of Light Alkanes. *Top. Catal.* **2013**, *56*, 1952−1962.
(45) Nguyen, T. T.; Deniau, B.; Delichere, P.; Millet, J. M. M. Influence of the Content and Distribution of Vanadium in the M1 Phase of the MoVTe(Sb)NbO Catalysts on Their Catalytic Properties in Light Alkanes Oxidation. *Top. Catal.* **2014**, *57*, 1152−1162.
(46) Chen, X.; Yang, Q.; Chu, B.; An, H.; Cheng, Y. Valence Variation of Phase-Pure M1MoVNbTe Oxide by Plasma Treatment for Improved Catalytic Performance in Oxidative Dehydrogenation of Ethane. *RSC Adv.* **2015**, *5*, 91295−91301.
(47) Chen, Y.; Qian, S.; Feng, K.; Li, Y.; Yan, H.; Cheng, Y. Determination of Highly Active and Selective Surface for the Oxidative Dehydrogenation of Ethane over Phase-Pure M1MoVNbTeO$_x$ Catalyst. *J. Catal.* **2022**, *416*, 277−288.
(48) Grasselli, R. K.; Buttrey, D. J.; Desanto, P.; Burrington, J. D.; Lugmair, C. G.; Volpe, A. F.; Weingand, T. Active Centers in Mo-V-Nb-Te-O_x (Amm)Oxidation Catalysts. *Catal. Today* **2004**, *91*, 251−258.
(49) Grasselli, R. K. Selectivity Issues in (Amm)Oxidation Catalysis. *Catal. Today* **2005**, *99*, 23−31.
(50) Wang, J.; You, R.; Zhao, C.; Zhang, W.; Liu, W.; Fu, X. P.; Li, Y. Y.; Zhou, F. Y.; Zheng, X. S.; Xu, Q.; Yao, T.; Jia, C. J.; Wang, Y. G.; Huang, W. X.; Wu, Y. E. N-Coordinated Dual-Metal Single-Site Catalyst for Low-Temperature CO Oxidation. *ACS Catal.* **2020**, *10*, 2754−2761.

https://doi.org/10.1021/prechem.4c00089
Precis. Chem. 2025, 3, 206−213

(51) Fu, C.; Li, F.; Yang, J. L.; Xie, J. J.; Zhang, Y. S.; Sun, X.; Zheng, X. S.; Liu, Y. X.; Zhu, J. F.; Tang, J. W.; Gong, X. Q.; Huang, W. X. Spontaneous Bulk-Surface Charge Separation of TiO_2-{001} Nanocrystals Leads to High Activity in Photocatalytic Methane Combustion. *ACS Catal.* **2022**, *12*, 6457−6463.
(52) Sun, X.; Chen, X.; Fu, C.; Yu, Q.; Zheng, X.-S.; Fang, F.; Liu, Y.; Zhu, J.; Zhang, W.; Huang, W. Molecular Oxygen Enhances H_2O_2 Utilization for the Photocatalytic Conversion of Methane to Liquid-Phase Oxygenates. *Nat. Commun.* **2022**, *13*, 6677.
(53) Yuan, Z.; Bai, Y.; Gong, K.; Huang, W. X. Accurate Measurements of NH_3 Differential Adsorption Heat Unveil Structural Sensitivity of Brønsted Acid and Brønsted/Lewis Acid Synergy in Zeolites. *J. Phys. Chem. Lett.* **2024**, *15*, 863−868.

https://doi.org/10.1021/prechem.4c00089
Precis. Chem. 2025, 3, 206−213